Viviani, M., Glisic, B., Scrivener, K. L., & Smith, I. F. C. "Equivalency points: Predicting concrete compressive strength evolution in three days" Cement and Concrete Research, 38(8-9), 2008, pp 1070-1078.

Equivalency Points: Predicting Concrete Compressive Strength Evolution in Three Days

M. Viviani[a*] B. Glisic[b], K.L. Scrivener[c], I. F.C. Smith[d]

---

[a] GCC Technology and Processes, Yverdon-les-Bains, Switzerland

[b] Smartec SA, Manno, Switzerland

[c] Ecole Polytechnique Fédérale de Lausanne (EPFL), Laboratoire des matériaux de construction (LMC)

[d] Ecole Polytechnique Fédérale de Lausanne (EPFL), Laboratoire d'informatique et de mécanique appliquées à la construction (IMAC)

ABSTRACT

Knowledge of the compressive strength evolution of concrete is critical for activities such as stripping formwork, construction scheduling and pre-stressing operations. Although there are several procedures for predicting concrete compressive strength, reliable methodologies involve either extensive testing or voluminous databases. This paper presents a simple and efficient procedure to predict concrete strength evolution. The procedure uses an experimentally-determined parameter called the *Equivalency Point* as

*Corresponding author: Marco Viviani, Av. des Sciences 1/A, Yverdon les Bains, Switzerland.
Email : mviviani@gcc.com

an indicator of equivalent degree of reaction. Equivalency Points are based on early age concrete deformation and temperature variations. Test results from specimens made from seven concrete types validate the approach.

Keywords: Strength Prediction, Hydration (A), Compressive Strength (C), Thermodynamic Calculations (B)

1 INTRODUCTION

A maturity method is used to predict the compressive strength evolution of concrete. Timely knowledge of such evolution helps to schedule operations such as pre-stressing and removal of formwork. The speed of construction can thus be increased using maturity methods without endangering safety. Such knowledge can also contribute to quality control. For example, the durability of structures is increased by avoiding excessive loading at early age.

The progress of hydration can be expressed by the degree of reaction α, expressed as the percent of the total product of reaction developed at a given time.

Maturity methods use functions of time and temperature to compute the progress of the hardening reactions. Semi-empirical formulas link the progress of reaction to strength. Values for the activation energy (E_a) and the rate of reaction (k) are necessary to implement the maturity approach when

equivalent time [1] is used as a function to calculate the progress of the hardening reaction. Determination of these values usually requires either extensive testing or large databases. In this paper, a simple and fast methodology to determine the activation energy E_a, the rate of reaction k_r (rate of reaction at a reference temperature T_r) and to predict compressive strength evolution is presented. This method also includes the determination of two other mixture-specific parameters necessary to model the evolution of compressive strength - the time at start of strength development (Et_0) and the ultimate compressive strength (S_u), strength at time $t=\infty$.

The Arrhenius equation can be used to determine the rate of a reaction when the value for activation energy, Ea, and a frequency factor, A, is known [2]. In order to reduce the number of unknowns, an alternative to the direct use of Arrhenius equation has been proposed. This is the maturity or Equivalent time (Et) (see Equation 1, [1]). Et is the integral in time of the ratio between the rates of reaction k = k (T) and $k_r = k(T_r)$ of two specimens of the same concrete type that are hardening at different temperatures. One is a virtual reference specimen that is assumed to be kept at a constant temperature T_r (generally 20 °C in Europe; 23 °C in USA). The other specimen is real and has a varying temperature T. R is the gas constant.

$$Et(t,T) = \int_{t_0}^{t} \left[\exp - \frac{Ea}{R} \left(\frac{1}{T} - \frac{1}{T_r} \right) \right] dt \qquad \text{Eq.1}$$

The equivalent time is of great interest for prediction of properties it allows comparison of concrete specimens that are hydrating at different rates. Among the formulas that link strength and equivalent time, the following semi-empirical relation is the most used. Equation 2 employs k_r and Et to predict the compressive strength [3].

$$S(k_r, Et) = S_u \frac{k_r \, (Et - Et_0)}{1 + k_r \, (Et - Et_0)} \qquad \text{Eq.2}$$

Carino and Lew have used successfully used this model for estimation of the 28-days strength [3]. To compute Et for a concrete, knowledge of the activation energy, E_a, is necessary (see Equation 1). Furthermore, to predict strength using Equation 2, k_r, Et_0 and S_u must also be known.

This paper describes a new methodology to determine E_a and k_r using early age measurements of deformations, temperatures and strengths. A methodology is also given for the determination of the parameters S_u and Et_0 in Equation 2, [5, 4]. These values are then used to predict the strength evolution in seven types of concrete covering a broad range of mix designs used in practice. The errors arising are analysed and a sensitivity analysis of the strength prediction is done for different values of the activation energy and the number of calibration points.

2 MEASUREMENT SYSTEM

Optical-fiber deformation sensors can be regarded as extensometers. They measure the deformation of the host material between the extremities of the gauge. They can be applied on the external surface of a structural member, as well as embedded in the material. Fiber optic sensors may have long or short gauge length. In general, Fabry-Perot and Michelson types are long gauge (>250 mm gauge length), while Bragg-grating types are short gauge (gauge length of few millimeters). All types can measure static and dynamic deformations. A long-gauge fiber-optic deformation sensor has recently been developed to measure deformation in fresh in concrete without being perturbed by the moisture of the

host material, temperature changes or magnetic fields [6]. The measurement system of the sensor is based on low coherence interferometry using single-mode optical fibers. The system includes a reading unit and fiber optic sensors. Figure 1 shows the system schematically. The reading unit is composed of a light emitter (LED), a low-coherence Michelson interferometer, completed with the optical devices used to carry, filter and analyze the light beams. The sensor consists of two single-mode optical fibers (called *measurement* and *reference* fiber). The measurement fiber is rigidly connected with the two anchor pieces and prestressed by 0.5%. Thus, it is able to follow the changes of length between the anchor pieces, both in traction and in compression. The stiffness of the sensor can be changed using stiffer or softer protection pipes. The reference fiber is glued to the anchor pieces but loose inside the protection tube (see Figure 2), hence the movement of the anchor pieces will not produce any changes of reference fiber length. Both fibers have, at one extremity, chemically deposed mirrors (see Figure 2). One of the two fibers is slightly shorter than the other, in order to create an "initial" interference path.

The Infrared light emitted by the LED passes through the optical fiber to the sensor, split (normally 50%-50%) by the coupler. The light moves along the reference and measurement fiber and is reflected by the mirrors, returning to the reading unit. Here the light generates an interference figure (see Figure 3) composed by a central and two lateral peaks.

This interference figure is analyzed (compensated) by the mobile mirror, and then sent to the PC. When no-deformation is imposed to the sensors, a fringe called "zero"-peak appears. The "zero" interference figure is created by the initial difference of length between the two fibres. When a deformation of the sensor occurs, the two lateral peaks displace, according to the change of the measurement fibre length

(see Figure 3). Performing the measurement takes less than 10 seconds. This sensor is particularly suitable for concrete, because of its robustness, temperature compensation, insensitivity to magnetic fields, and a precision of 2 μm. Moreover, such sensors can follow the deformation of fresh concrete without disturbing the strain field of the host material [7]. The stiffness and the thermal expansion coefficient (TEC) of the sensors are influenced mainly by the characteristics of the protective tube.

Glisic proposed a Michelson sensor called a “setting” sensor with a high axial stiffness because it was housed in a tube made of stainless steel [7, 8]. In this work a “soft sensor” and “stiff sensor” were used, which are Michelson sensors packaged into a soft plastic pipe (soft sensor) and in a steel pipe (stiff sensor) respectively. The different types of packaging (casing) provide a different axial stiffness of the sensors. The soft sensor has a very low stiffness because it is housed in a soft plastic tube and for this reason the soft sensor measures the deformations of the concrete matrix from very early times, as soon as the stiffness of the concrete specimen overtakes the sensor stiffness. The Stiff sensor is similar to the setting sensor or Glisic [7,8], differing only in the type of pipe used and the assembly system. The assemblage of Stiff and Soft sensors is shown in Figure 4. Soft and Stiff sensors have equal gauge length

The stiff sensor, once embedded in concrete, together with a soft sensor of the same gauge length, leads to determination of a difference curve between the deformation measured by the two sensors. When concrete is placed, the soft sensor measures the swelling (or contraction) of the concrete (because it is very soft) while the stiff sensor is initially not influenced by the deformations of the concrete matrix and therefore the difference between deformations measured by the two sensors increases and then

decreases [4]. When the difference becomes constant, this is called the “hardening point” and in a previous article [5] this alone was used to predict 3-day strengths.

In this paper, the methodology is made more versatile by dividing the difference between the sensors by the variation in temperature in order to account for measurement bias due to temperature; as the shape of the difference curve is dependent on the temperature variation–time history. These curves always show a steep increase and then level off to a constant value (see Figure 5). Later, as the delta temperature or deformation approaches zero there is a vertical asymptote. The point at which a line drawn on the plateau of the $\frac{\Delta\varepsilon_{st-soft}}{\Delta T}$ curve departs from the curve on the left side is defined as the *equivalency point*. This point on the curve is assumed to occur at the same α (degree of reaction) and is the basic assumption of this method for calculating activation energies.

3 EXPERIMENTAL AND CALCULATION

3.1 Determination of the activation energy E_a

The strategy adopted for determining the activation energy uses two specimens of the same concrete. It is based on the determination of the equivalency point of these two specimens. Both specimens have the same dimensions. They are both monitored with a stiff and a soft sensor. Each pair of sensors has the same features. One specimen is wrapped with glass wool. The glass wool acts as insulation and

keeps the temperature of this specimen at a higher level than the temperature of the other specimen. The rate of reaction in the insulated cylinder is therefore higher. The temperature is measured in both specimens (see Figure 6). The specimens are cured under sealed conditions – no moisture exchange with the environment. The degree of reaction, in terms of equivalent time (Et), can be calculated by Equation 1. For the specimens under sealed conditions the deformation of the concrete, ε_{conc}, is the sum of the autogenous (ε_{aut}) and thermal (ε_{th}) deformations:

$$\varepsilon_{conc} = \varepsilon_{aut} + \varepsilon_{th} = \varepsilon_{aut} + TEC_c * \Delta T \quad \text{Eq.3}$$

The soft sensor measures the deformation of the concrete matrix from very early age because of its low axial stiffness [7, 8]. It is assumed that the stiff sensor measures a part of the deformation of concrete that is a function of the degree of reaction [7]. So the dependence of the deformation of the stiff sensor on the degree of reaction is expressed by a transfer coefficient $\aleph = \aleph(\alpha)$ which accounts for the percentage of deformation that the interface transfers to the sensor. Thus, the deformation transferred from the concrete to the stiff sensor, $\varepsilon_{conc \rightarrow st}$ can be expressed as follows:

$$\varepsilon_{conc \rightarrow st} = \aleph * (\varepsilon_{conc}) \quad \text{Eq. 4}$$

However, the stiff sensor also changes its length according to the thermal expansion coefficient of the casing (steel in this case), TEC_s and to the temperature change (see Figure 7):

$$\varepsilon_{steel} = TEC_s * \Delta T \quad \text{Eq. 5}$$

Because the stiff sensor and the hardening material have different and (in the case of concrete) changing thermal expansion coefficients, the changing temperature produces additional differences in deformation, termed here thermal interaction deformation ε_{ti}. This thermal interaction deformation is

proportional to the difference of thermal expansion coefficients of the two materials (steel and concrete), K. This effect is also influenced by the transfer coefficient. Thus, this deformation is measured by the stiff sensor with a magnitude proportional to the transfer function $\aleph = \aleph(\alpha)$:

$$\varepsilon_{ti \to st} = \aleph * (K * \Delta T) \quad \text{Eq. 6}$$

Therefore, the total deformation measured by the stiff sensor is the sum of the terms in Equations 4-6:

$$\varepsilon_{st} = \aleph * (K * \Delta T + \varepsilon_{aut} + TEC_c * \Delta T) + TEC_s * \Delta T \quad \text{Eq. 7}$$

The difference between the deformation measured by the soft and the stiff sensor is determined by Equation 9:

$$\begin{cases} \varepsilon_{soft} \approx \varepsilon_{conc} = \varepsilon_{aut} + TEC_c * \Delta T \\ \varepsilon_{st} = \aleph * K * \Delta T + \aleph * \varepsilon_{aut} + \aleph * TEC_c * \Delta T + TEC_s * \Delta T \end{cases} \quad \text{Eq. 8}$$

$$\Delta\varepsilon_{st\text{-}soft} = \aleph * K * \Delta T + (\aleph - 1) * \varepsilon_{aut} + (\aleph - 1) * TEC_c * \Delta T + TEC_s * \Delta T \quad \text{Eq. 9}$$

In Equation 9, the term $\Delta\varepsilon_{st\text{-}soft}$ (t) is the hardening curve [4]. Dividing both sides of Equation 9 by ΔT the following equation is obtained:

$$\frac{\Delta\varepsilon_{st\text{-}soft}}{\Delta T} = \aleph * K + \frac{(\aleph - 1)}{\Delta T} * \varepsilon_{end} + (\aleph - 1) * TEC_c + TEC_s \quad \text{Eq.10}$$

It is assumed that at a certain degree of reaction ($\alpha = \alpha^*$) – the ***Equivalency Point*** – the deformation is fully transferred to the stiff sensor (non slip point), i.e. that $\aleph(\alpha*) = 1$, in which case equation 10 becomes:

$$\frac{\Delta\varepsilon_{st\text{-}soft}}{\Delta T} = K + TEC_s \qquad \text{Eq. 11}$$

In Equation 11 the value of $\frac{\Delta\varepsilon_{st\text{-}soft}}{\Delta T}$ becomes a constant when K becomes constant. Since the thermal expansion coefficient of steel is constant in time, the coefficient K is constant when the thermal expansion coefficient of the hardening material is constant. When K is constant Equation 11 describes a horizontal line on a plot of $\frac{\Delta\varepsilon_{st\text{-}soft}}{\Delta T}$ versus time. A further analysis of Equation 11 indicates the possible shapes of the experimental curves. Two situations might occur:

$\Delta\varepsilon_{st\text{-}soft} \neq 0$
$\Delta T \neq 0$ → the curve will level off to a constant value
$\aleph = 1$

$\Delta\varepsilon_{st\text{-}soft} = 0$
$\Delta T = 0$ →a vertical asymptote will appear
$\aleph = 1$

The two situations are shown in Figure 5.

The *Equivalency Point* occurs at a constant degree of reaction for the same hardening material. This assumption is valid under two conditions. The first is that $\aleph = \aleph(\alpha)$; i.e. the interfacial bond strength, is a function of the degree of reaction. This assumption is supported by the literature which indicates that the characteristics of interfaces between bars or fibers and cement-based materials evolve with the degree of reaction [9, 10, 11]. The second assumption is that K (or the TEC of concrete) becomes constant. Few results have been found concerning the evolution of thermal expansion coefficient of concrete in term of degree of reaction [12, 13, 14, 5, 15]. However many researchers agree to define

the TEC_c as a function of the degree of reaction. The Equivalency Point usually appears in the first 10–30 hours of equivalent time, in the zone where $\Delta\varepsilon \neq 0; \Delta T \neq 0$.

The definition of Equivalency Point can be used to extract the activation energy E_a from hardening measurements. If two specimens of the same concrete are monitored with stiff, soft and temperature sensors but with different temperature regimes (Figure 8), the equivalency point can be determined for each specimen. For both specimens the Equivalency Point occurs at the same equivalent time (maturity). Temperature profiles are inserted in Equation 1 for each specimen and the integral is calculated to the Equivalency Point. This results in two equations with two unknown values (Et and E_a) which can be solved. The values are shown in Table 1.

3.2 Determination of the zero equivalent time

The Zero equivalent time, Et_0 in Equation 2 is the time at which strength development starts. Conventionally this could be taken as the setting time, but as the setting time is somewhat arbitrary and would require separate measurement; here we take it as the point when the self heating of the concrete starts, which is equivalent to the start of the acceleration of hydration leading to hardening. This point can be extracted from the data acquired during the tests, by study of the temperature curves. Before the hydration reaction starts to accelerate the temperature of the concrete is influenced by the ambient temperature. During this period three situations may occur depending on the temperature difference between the mixed concrete and its surroundings.

a. Heating;
b. Constant temperature; and
c. Cooling.

Situation (a) is very unlikely and was never seen in this work, but Et_0 can in any case be detected from the upturn of the temperature curve (case 1, Figure 9). In Situation (b) Et_0 can also be detected when the temperature shows a sharp increase (case 2, Figure 9). The third situation is the most difficult. Cooling occurs as a consequence of lower external temperature and can be assumed to be linear in the first hours. The moment when fast hydration begins was therefore taken as the moment when the temperature curve loses its linearity (see Case 3 in Figure 9). This methodology is directly related to what occurs in each pour of concrete and was found to be more relevant than determining the setting time at a reference temperature and taking this as the Et_0 for all the pours of the same concrete. This method avoids the need for separate measurements and also allows the effect of chemicals (such as plasticizers) on the rate of reaction to be taken into account. Results for the 7 concretes studied are reported in Table 1

3.3 Determination of Su and k_r.

Quantification of the activation energy is necessary but not sufficient for predicting strength. The prediction of the compressive strength evolution is possible if two calibration compressive strength tests are conducted at different Equivalent times using standard specimens of the same composition, humidity, boundary conditions and known temperature histories. This allows the values of k_r and Su to be determined. In this article these two calibration strength tests are indicated on the graphs. Values for Su and k_r can be obtained using strength tests at any time; in this work the Calibration tests were carried out at 48 hours and 72 hours after casting. The Equivalent age at the time of the calibration tests was evaluated using the activation energy determined as described in Section 3.1 and the temperature history of the specimen. The zero equivalent time is obtained using the methodology described in

Section 3.2. For the two tests the strength, the equivalent time and the zero equivalent time are inserted in Equation 2. This gives two equations which can be solved for the two unknowns (k_r and Su). To further verify the results further calibration strength tests can be used to obtain multiple values for k_r and Su. The new or average values for k_r and Su can be used for a new prediction. Every strength test can be a used as an additional calibration point. In this study the 7-days strength was used as a third calibration test for the analysis of errors. The 24-hour test was not been found to be an appropriate calibration test this may be because the concretes have a 24-hour strengths under standard condition that is close to the lower limit of the testing range and so more variable.

3.4 Tests

Activation energies, k_r, Su and Et_0 were evaluated and applied to seven different types of concrete detailed in Table 2 using the procedure presented above. Five were commonly used concrete types in civil engineering. They were made with different types of aggregate. Air entrainers, superplasticizers and different types of cement (see Table 2). The predicted strength evolution curves shown in Figures 10-16 were obtained from calibration strengths obtained within the first 72 hours. The predictions obtained were compared to the criteria given by the Texas Department of Transportation code (TEX-426-A, see Table 3) which was the most stringent found in the literature. They were found to be realistic and acceptable without any correction according to this criteria (see Tables 3 and 4). The quality of the prediction was verified after 7, 21 and 28 days (with exception of Test 7, for which test at 21 days is not available). Times of strength testing were 2, 3, 7, 21 and 28 days actual elapsed time and not equivalent time. The maximum deviation between predicted and tested values of each test is presented in Table 4. A comparison with values determined with the earlier method using hardening times [5] show that the results are essentially similar, but with slightly lower maximum error (6.2 % in comparison to 7.4%). It is also important to note that this method based on the determination of

equivalency points is faster and more automated evaluation of the activation energy than determination of hardening times.

3.4 Estimation of errors

Values for equivalent time are determined using equivalency points (see section 3.1). Equivalency points are determined using measurement of temperature and deformation. Errors affecting measurement thus affect values for activation energy and subsequently, strength predictions.

Measurement errors have been estimated for deformation and temperature using experimental values. Measurement noise when reading deformation and temperature as well as time dependent drift are especially important when deformation and temperature readings are added, subtracted multiplied or divided since errors can amplify to become high percentages of results that are reported. Propagation of errors has been estimated in order construct the error envelope for TEC (and for autogenous deformation). The error, Δs, for addition and subtraction of quantities A and B is calculated as follows:

$$\Delta s = \sqrt{\Delta A^2 + \Delta B^2} \quad \text{Eq.12}$$

Where:

Δs= error related to results of addition or subtraction of quantities A and B

ΔA= error related to measuring quantity A

ΔB= error related to measuring quantity B

For multiplication and division of quantities A and B the error is calculated as follows:

$$\Delta r = \sqrt{\left(\frac{\Delta A}{A}\right)^2 + \left(\frac{\Delta B}{B}\right)^2} \quad \text{Eq.13}$$

Δr= error related to results of multiplication or division of the quantities A and B

The equivalency point is assumed to relate to a certain degree of reaction. This assumption is made on the basis of the mechanism of deformation transferring between the hardening material and sensors. This means that at the equivalency point, the degree of reaction is the same for all specimens of the same material, hydrating in autogenous conditions. This equivalency is independent of the combination of time and temperature that has lead to such a degree of reaction.

Determination of E_a requires detection of the equivalency point. Errors in the determination of the equivalency point might result in poor predictions of activation energy. Drift and noise related to measurements introduce an error in terms of time on the equivalency point. The worst case scenario for the calculation of the activation energy corresponds to a bound of ± 6 minutes on values for the equivalency points. This leads to two values for bounds on the activation energy. The worst case scenario on the value for the activation energy has been considered. The variation of the activation energy has an effect on values calculated for strength evolution. The effect of the activation energy variation in strength is shown in Table 5 for predictions made using two calibration times and Table 6 for prediction made using three calibrations times (2, 3 and 7 day strengths). Tables 5 and 6 show that, despite propagation of the errors on measurements, prediction fits in all cases the requirements for prediction of code TEX 426 A (except Test 1, two calibration times, upper bound E_a value). These show the robustness of the methodology.

4 DISCUSSION

The methodology presented here assumes that the Equivalency Point is an indicator of the degree of reaction. The good predictions obtained support this assumption for the range of concretes studied. Constraints on the testing procedure (such as minimum difference in temperature profiles) could be added for a better definition of hardening time where necessary. The relationship between the hardening curve and the degree of reaction is an important issue for the extension of the methodology to the general field of hardening materials and this will be the subject of further study. The basis of the proposed methodology allows the thermodynamic-chemical properties (activation energy and rate of reaction) to be determined and converted to compressive strength via calibration tests. Codified methods use similar concepts by inserting the final setting time into maturity-strength equations and performing regression analyses.

Currently, maturity methods are still rarely used in practice. This lack of acceptance is partially related to limited practical experience and the extensive prior testing needed for calibration of classical methods. Confidence in the methodology presented here would be increased through performing more compressive tests during the early age of concrete. For example, using a given pair of compressive-strength values, the value of k_r and Su are obtained, and a predictive curve can be calculated. Using other pairs, an envelope of curves is obtained. A standard apparatus for the application of this

methodology is under development. Since the apparatus is reusable and robust, an inexpensive and in-situ application of the methodology is feasible.

5 SUMMARY AND CONCLUSIONS

Compressive strengths of several widely used concrete mixes have been successfully predicted using a procedure that involves early age deformation monitoring. The procedure has also been applied to a special concrete in order to study the applicability of the methodology to other types of hardening materials. This methodology allows a fast and accurate prediction of values for compressive strength on site. Common methods for estimation of in place strength requires extensive use of curing of mortar cubes at constant temperatures or the use of databases containing a large number of compressive strength values made at many ages and cured at different temperatures. These databases have to be fed with a statistical relevant number of data before a reliable estimation of the strength can be made. Furthermore all of these methods requires many hours of lab and field time for testing, collecting and analyzing data. The method here allows strength to be *predicted* from concrete monitored in situ and early calibration strengths of test specimens from the same batch of concrete – i.e no prior testing is necessary. All the data can be obtained from specimens cast at the same time and from the same batch as the concrete used on site. Seventy-two hours are sufficient to gather data and predict strength evolution with less than 7% error. Common maturity methods cannot estimate the 28-day strength of a mixture without having a prior set of data on 28-day strength of such mix. The new methodology, presented here based on equivalency points is more flexible and gives lower errors compared to the

previously presented method based on hardening time [5]. The method also provides explicit values for the activation energy and the rate of reaction.

6 ACKNOWLEDGEMENTS

This project was supported in its early stages through a project funded by the Swiss Commission for Technology and Innovation (CTI) and Cemsuisse (Swiss Cement Fabricators Association). The authors express special thanks to Patrice Gallay who has helped design and build testing apparatus.

7 NOTATION

α Degree of reaction (% of the total product of the reaction)
k Reaction rate h^{-1}
k_r Rate of reaction at the reference temperature T_r
R Gas constant ($KJ*mole^{-1}* K^{-1}$)
T Temperature (K)
T_r Reference temperature (K)
ΔT change in temperature.
Et_0 Equivalent time at start of strength development (hours)
Et Equivalent time (hours)
S Compressive strength at age t (MPa),
S_u Ultimate compressive strength (strength at time $t=\infty$),
t Time (hours)
t_0 Age at start of strength development (hours)
ε_{conc} concrete deformation;
ε_{soft} soft sensor deformation;
ε_{st} stiff sensor deformation;
ε_{aut} concrete autogenous deformation;
ε_{steel} steel deformation;
$\varepsilon_{conc\rightarrow st}$ deformation transferred from the concrete to the stiff sensor;
$\varepsilon_{r\rightarrow st}$ thermal interaction deformation transferred from concrete to stiff sensor; and
$\aleph$ Function dependent on the degree of reaction;

TEC_c concrete thermal expansion coefficient;
TEC_s steel thermal expansion coefficient; and
K constant depending on steel and concrete TEC
E_a Activation energy (KJ/mole)
A Frequency factor (s^{-1})

8 REFERENCES

[1] Freiesleben Hansen, P. and Pedersen J., Maturity computer for controlled curing and hardening of concrete**,** Nordisk Betong, 1 (1977), 19-34.

[2] Arrhenius, S., On the reaction velocity of the inversion of cane sugar by acids**,** Zeitschrift für Physikalische Chemie 4 (1889), 226-232. [as translated and published in Margaret H. Back & Keith J. Laidler, 1967, "Selected Readings in Chemical Kinetics" Pergamon, Oxford 1967]

[3] Carino N.J. and Lew H.S., The maturity method: from theory to application, Proceedings of the 2001 Structures Congress & Exposition, Washington, D.C., ASCE, Reston, Virginia, Peter C. Chang, Editor, (2001), 19 p.

[4] Viviani, M., Monitoring and modeling of construction materials during hardening, Doctoral Thesis No. 3168, EPFL, Lausanne, Switzerland, 2005, 172 p.

[5] Viviani, M., Glisic, B. and Smith, I. F.C., Three-day prediction of concrete compressive strength evolution, ACI materials J. 102 (4) (2005) 231-236.

[6] Inaudi, D., Fiber optic sensor network for the monitoring of civil engineering structures, Ph.D. Thesis No. 1612, EPFL, Lausanne, Switzerland, 1997.

[7] Glisic, B., Fibre optic sensors and behaviour in concrete at early age**,** Ph.D. Thesis, N°2186, EPFL, Lausanne, Switzerland, 2000.

[8] Glisic B., Simon N., Monitoring of concrete at very early age using stiff SOFO® sensor, Cement and Concrete Composite 22 (2) (2000) 115-119.

[9] Chan Y., Li V., Age effect on the characteristics of fibre/cement interfacial properties, Journal of Materials Science 32 (19) 1997, 5287-5292.

[10] Holshemacher, K., Weisse, D., Klotz, S., Bond of reinforcement in ultra high strength concrete, proceedings, International symposium on ultra high performance concrete, September 13-15, Kassel, Germany, 2004, pp. 375-387.

[11] Delatte, N. J., Fowler, D. W. and Williamson, M. S., Bond strength development with maturity of high-early-strength bonded concrete overlays, ACI Materials J. 97 (2) 2000 201-207.

443 [12] Turcry P., Loukil A., Barcelo L. and Casabonne J. M., Can the maturity concept be used to
444 separate the autogenous shrinkage and thermal deformation of a cement paste at early age?, Cement
445 and Concrete Research 32 (9) 2002 1443–1450.
446
447 [13] Laplante P., Boulay C., Evolution du coefficient de dilatation thermique du béton en fonction de
448 sa maturité aux tout premiers âges, Materials and Structures 27 1994 596-605
449
450 [14] Bjøntegaard, Ø., Thermal dilation and autogenous deformation as driving forces to self-induced
451 stresses in high performance concrete, Ph.D. Thesis, The Norwegian University of Science and
452 Technology, N-7491 Trondheim, Norway, 1999.
453
454 [15] Bjøntegaard, Ø., Sellevold E., Interaction between thermal dilation and autogenous deformation in
455 high performance concrete, Materials and Structures 34 2001 266-272.
456

9 FIGURES and TABLES

Table 1, Values for t_0, Ea, k_r, S_u and E_t at the equivalency point for the 7 types of concretes studied.

Test number	Initial time t0 (h)	Ea J/mol	k_r h^{-1}	S_u MPa	Et at the equivalency point, (hours at 20°C)
Test 1	2.7	39000	.0147	43.0	14.45
Test 2	2.2	28100	.0441	37.9	25.3
Test 3	4.0	27000	.0198	51.0	18.1
Test 4	2.5	42600	.0090	46.9	15.55
Test 5	0	36600	.0213	35.7	15.75
Test 6	22.75	25500	.0321	182.8	49.85
Test 7	1.25	36500	.0289	53.5	13.4

Table 2 Mix-design test 1-7

	Test 1	Test 2	Test 3	Test 4	Test 5	Test 6	Test 7
Water/cement Ratio	0.45	0.45	0.48	0.48	0.48	0.18	0.43
Cement type	CEM II / A-LL 42.5 R	CEM I 42.5 R	CEM I 42,5 N HS	CEM III/A 32,5 N	CEM II/ A-LL 32.5 R	CEM I 52,5 N HTS	-
Cement	325 Kg/m3	350 Kg/m3	360 Kg/m3	360 Kg/m3	360 Kg/m3	1051.1 Kg/m3	420 Kg/m3
Superplasticizer	0.9%	0.8%	0.8%	0.8%	0.8%	35.1 kg/m^3	No
Air Entrainer	0.1%	-	-	-	-	-	-
Aggregate	0-32 Hüttwangen	0-32 Sergey	0-32 Sergey	0-32 Sergey	0-32 Sergey	0-4 Sand of Fontainebleau	0-32 Sergey
Silica fume	-	-	-	-	-	273.3 Kg/m^3	No
Steel fibre	-	-	-	-	-	Yes*	No
Max. temperature difference	5 °C	15 °C	20.2 °C	14.5 °C	21.6 °C	14.5 °C	30 °C

Table 3 Verification criteria for maturity prediction; code TEX-426-A. s = predicted strength, s* = independent test results.

Verification criteria	Adjusting procedure
$s^* \leq 0.90\ s$ $s^* \geq 1.10\ s$	Develop new S-M relationship
3 consecutives within $0.90\ s \leq s^* \leq 0.95\ s$ $1.05\ s \leq s^* \leq 1.10\ s$	Evaluate batching and placement adjust s-M relationship if needed
Better correlations	S-M relationship accepted

Table 4 Maximum error between predicted strength and independent test results for the methodology proposed in this paper (equivalency points) and for a previous proposal using hardening times [4]

	Maximum Errors			
Test	Day of occurrence of max. error	Maximum error % (equivalency points)	Day of occurrence of max. error	Maximum error % (hardening times)
1	21	**+6.2 %**	7	+4.5 %
2	28	-6.0 %	28	-5.1 %
3	28	+5.8 %	28	+5.1 %
4	21	-6.1 %	21	**-7.4 %**
5	28	-5.1 %	28	-6.4 %
6	30	+3.8 %	13	+3.7 %
7	28	+1.3%	8	-

Table 5 Effect of the variation of the activation energy on the predicted strength (two calibration points)

Test number	Activation energy J/mol		k_r h^{-1}	S_u MPa	$\frac{\text{Predicted strength - Average test strength}}{\text{Average test strength}} \bullet 100$		
					7th day	21st day	28th day
Test 1	+	53250	.0162	41.2	-6.5	-3.5	-10.2
	mid	39000	.0147	43.0	-5.4	-1.0	-6.2
	-	28200	.0158	41.4	-4.5	0.8	-3.6
Test 2	+	37400	.0393	38.3	4.1	3.4	5.3
	mid	28100	.0441	37.9	4.4	4.1	6.0
	-	20600	.0483	40.0	4.6	4.6	6.6
Test 3	+	31500	.0202	50.7	-1.7	0.3	-5.3
	mid	27000	.0198	51.0	-1.9	-.2	-5.8
	-	23300	.0195	51.2	-2.0	-0.4	-6.1
Test 4	+	48800	.0090	47.8	1.3	5.1	1.9
	mid	42600	.0090	46.9	1.3	6.1	3.2
	-	36900	.0090	46.1	1.3	7.0	4.3
Test 5	+	40000	.0209	35.9	-1.5	0.9	4.7
	mid	36600	.0213	35.7	1.3	1.2	5.1
	-	26000	.0204	36.2	0.9	0.5	4.2
Test 6	+	27900	.0312	183.8	-4.1	-2.3	0
	mid	25500	.0321	182.8	-3.8	-1.9	.4
	-	24000	.0326	182.1	-3.6	-1.7	.7
Test 7	+	53450	.0253	55.0	.6	-	-2.1
	mid	36500	.0289	53.5	1.3	-	-.2
	-	24000	.0317	52.6	2.1	-	1.2

Table 6 Effect of the variation of the activation energy on the predicted strength (three calibration points)

Test number	Activation energy J/mol		k_r h^{-1}	S_u MPa	$\frac{\text{Predicted strength - Average test strength}}{\text{Average test strength}} \bullet 100$	
					21st day	28th day
Test 1	+	53250	.0162	41.2	-.7	-4.3
	mid	39000	.0173	39.8	1.8	-1.3
	-	28200	.0181	38.9	3.4	0.7
Test 2	+	37400	.0339	40.2	0.3	1.8
	mid	28100	.0377	39.9	.4	2.1
	-	20600	.0409	39.7	.5	2.3
Test 3	+	31500	.0208	50.1	1.2	-4.3
	mid	27000	.0209	50	1.4	-4.1
	-	23300	.0212	49.8	1.6	-3.8
Test 4	+	48800	.0086	49.4	2.8	-.7
	mid	42600	.0086	48.5	3.9	.7
	-	36900	.0090	47.7	4.9	1.9
Test 5	+	40000	.0202	36.2	.5	4.3
	mid	36600	.0204	36.1	.7	4.5
	-	26000	.0199	36.3	.3	4.1
Test 6	+	27900	.0355	177.1	.7	3.1
	mid	25500	.0361	176.6	.8	3.3
	-	24000	.0365	176.3	.9	3.4
Test 7	+	53450	.0248	55.4	-	-2.8
	mid	36500	.0276	54.4	-	-1.5
	-	24000	.0296	53.9	-	.9

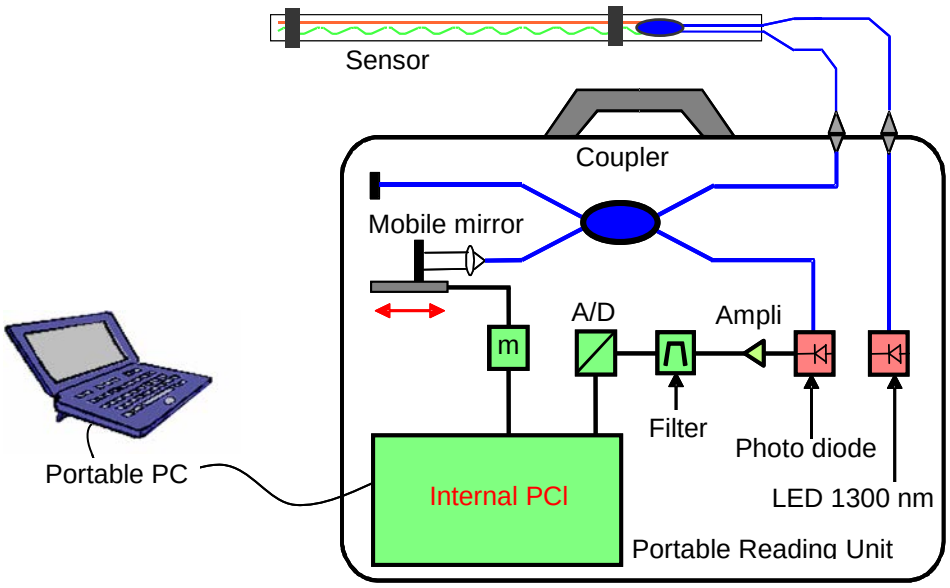

Figure 1 The SOFO monitoring system set-up

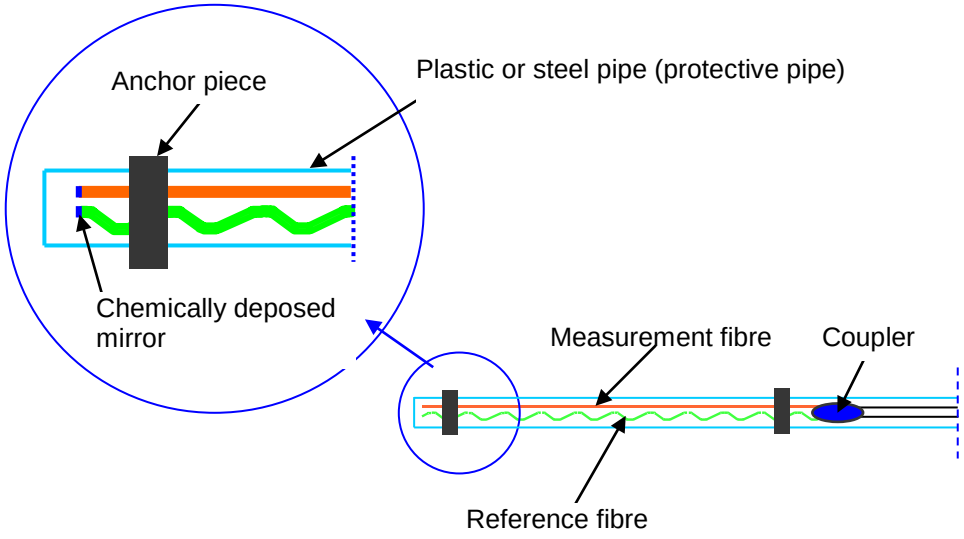

Figure 2 A general scheme of the SOFO sensor

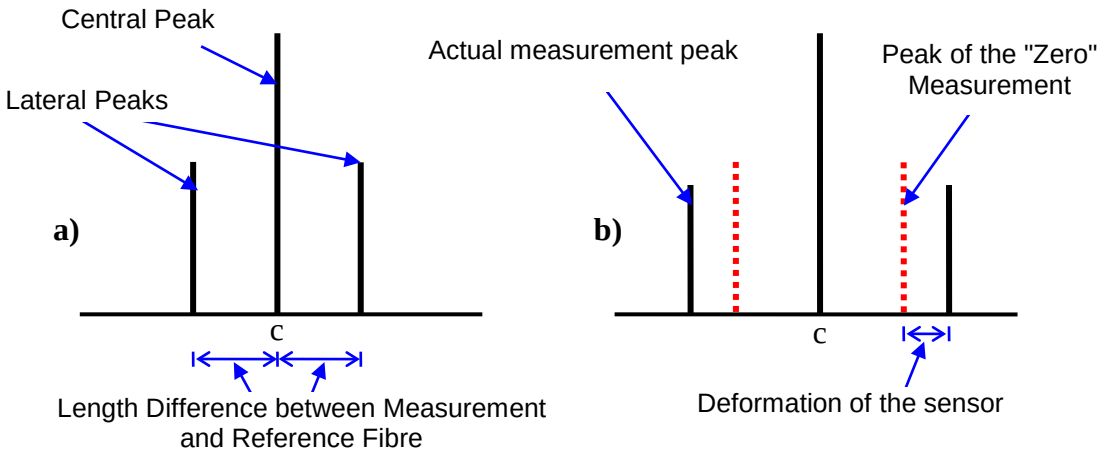

Figure 3 A scheme of the SOFO measurement representation

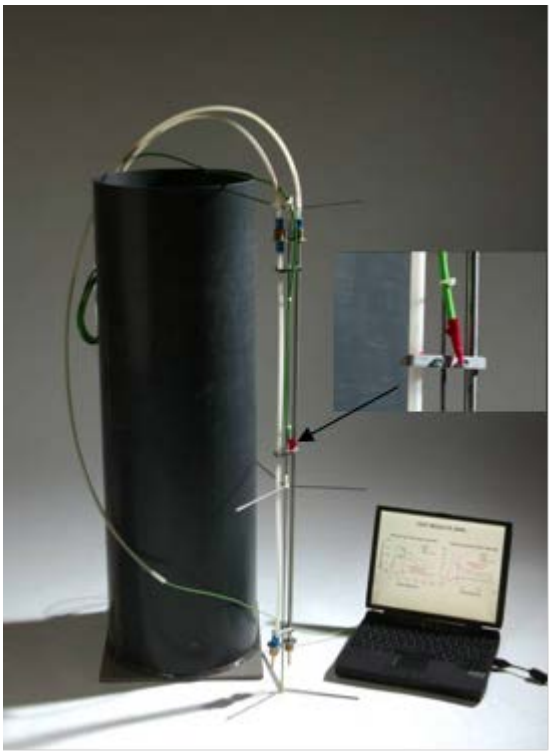

Figure 4 The soft and stiff SOFO sensors. [3]

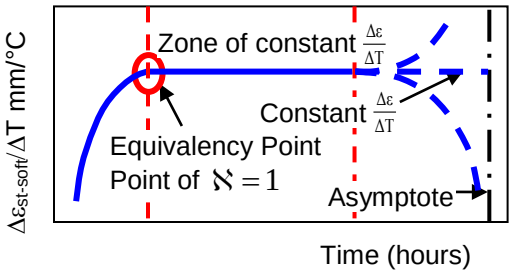

Figure 5 Predicted shape of the $\frac{\Delta\varepsilon_{st\text{-}soft}}{\Delta T}$ curve

496
497
498

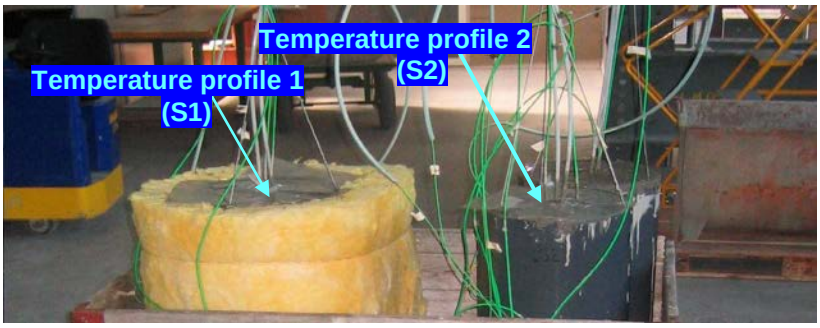

Figure 6 Specimens under test

499
500

Figure 7 Reaction deformation

501
502

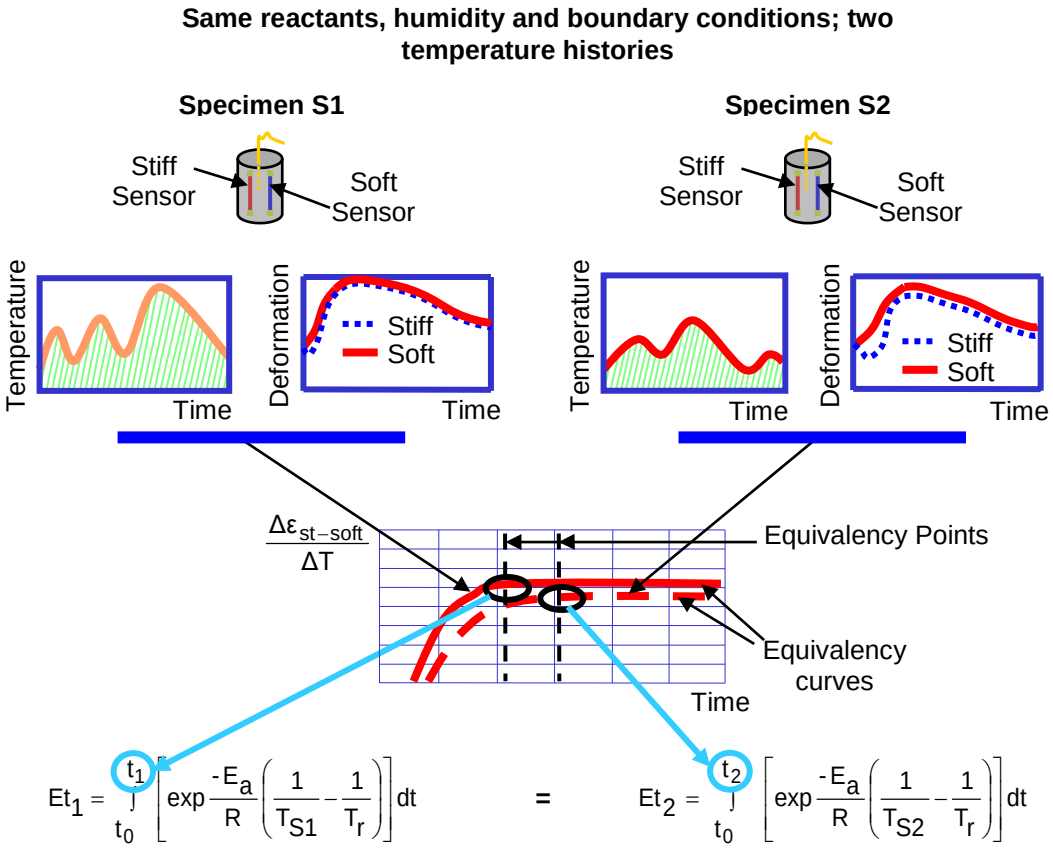

Figure 8 Determination of the activation energy E_a

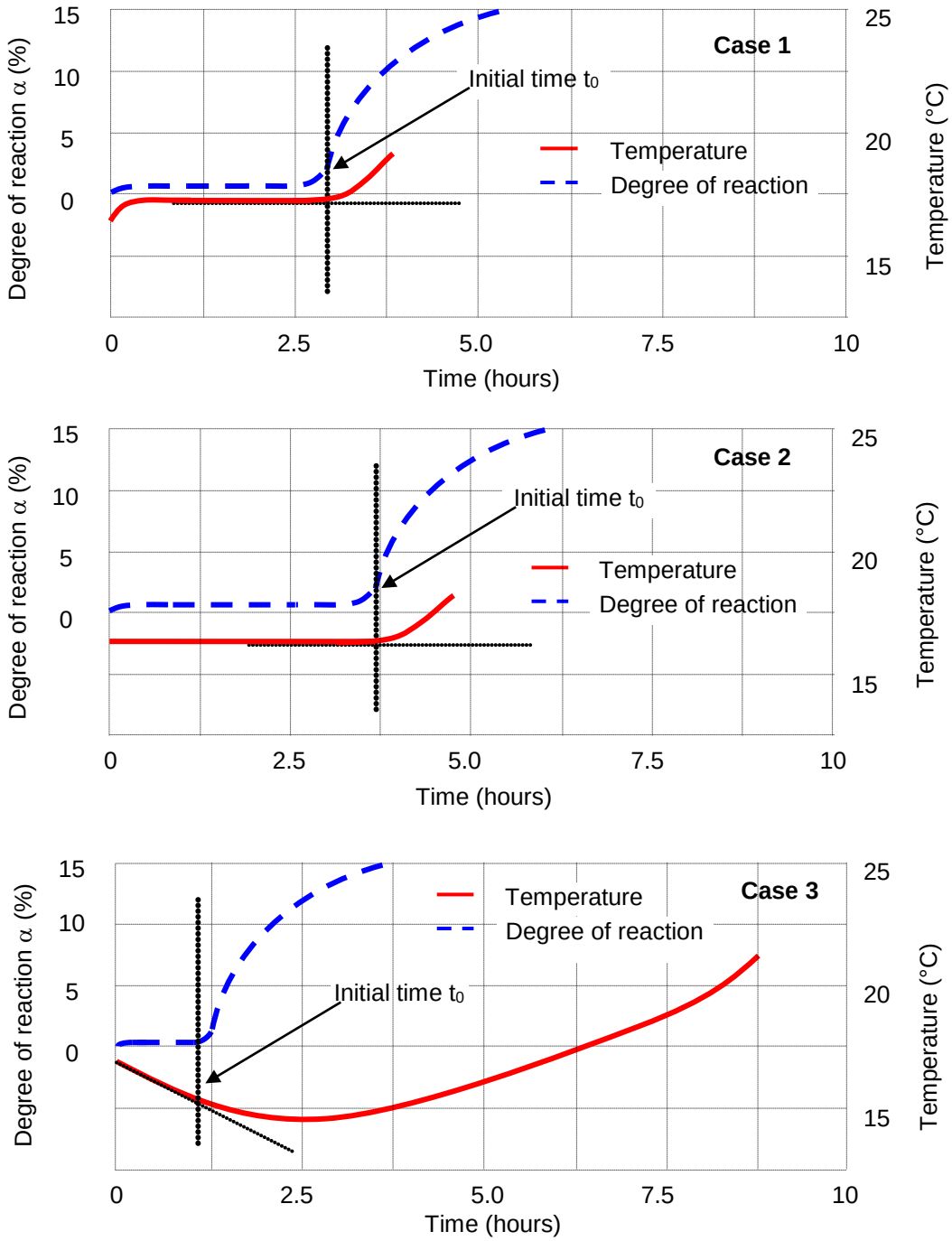

Figure 9 Determination of the time of the Determination of the zero equivalent time

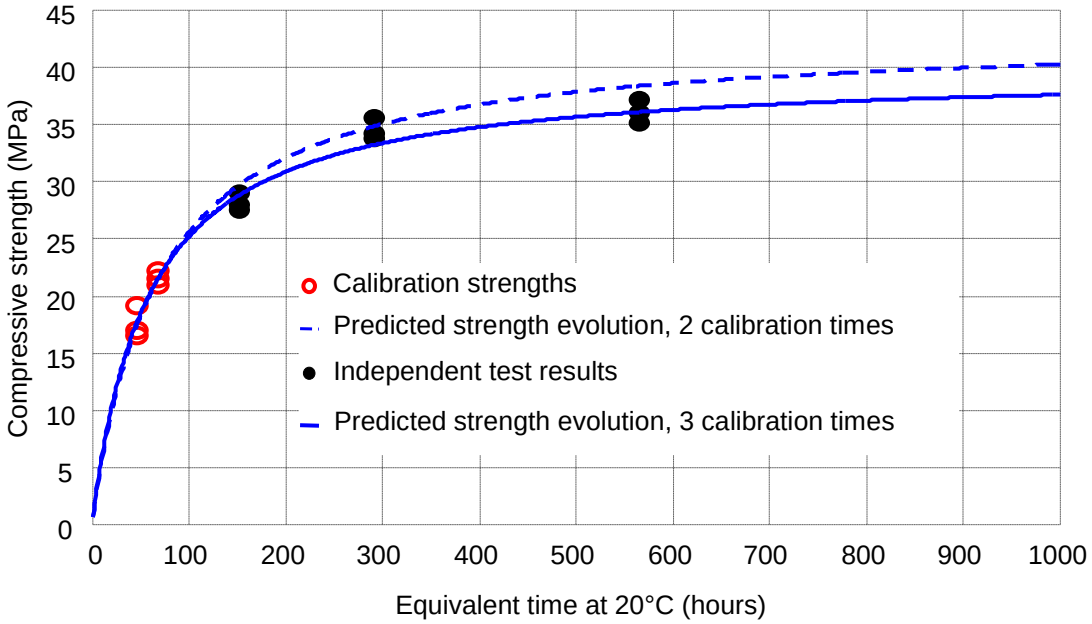

Figure 10 Compressive strength vs. equivalent time for test series 1. Calibration strengths of young concrete are used to predict strength evolution and this prediction is verified by independent test results using cylinders containing more mature concrete.

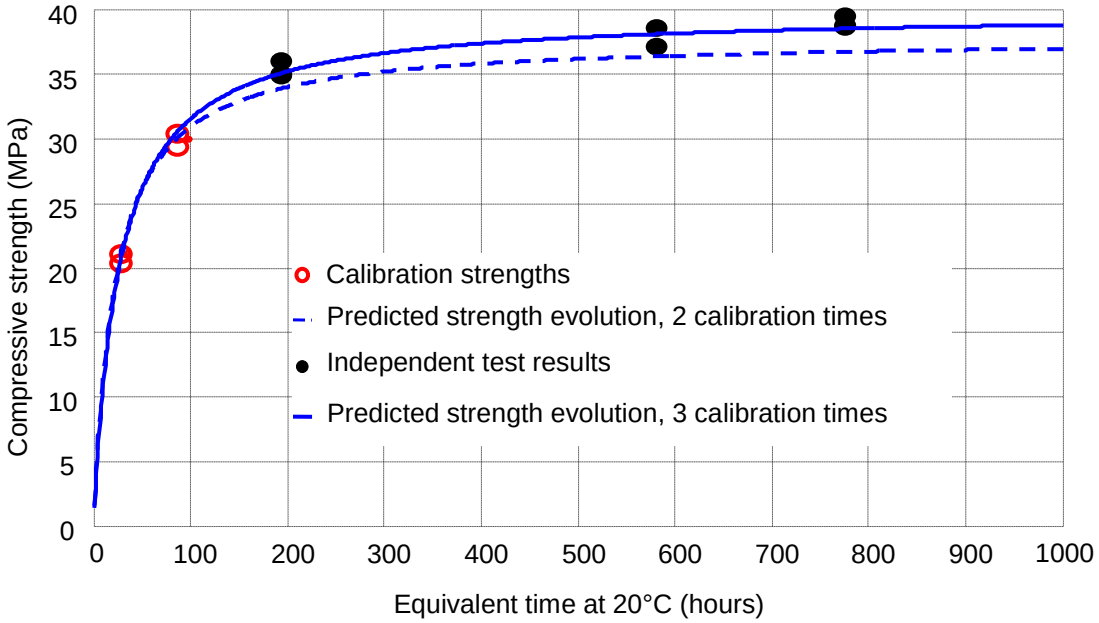

Figure 11 Compressive strength vs. equivalent time for test series 2. Calibration strengths of young concrete are used to predict strength evolution and this prediction is verified by independent test results using cylinders containing more mature concrete.

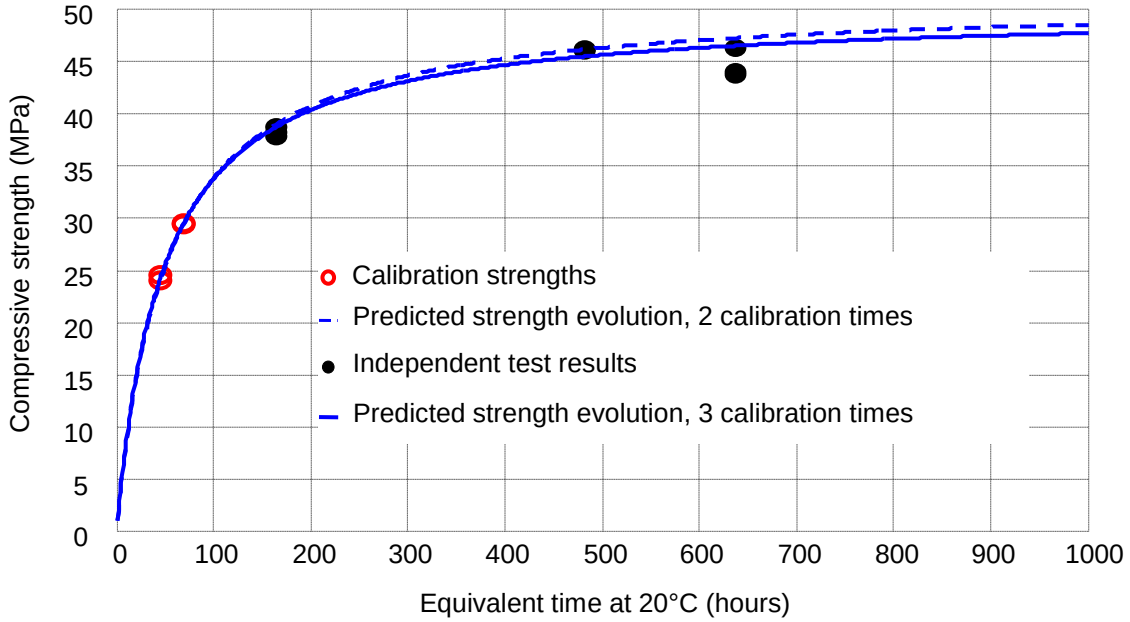

Figure 12 Compressive strength vs. equivalent time for test series 3. Calibration strengths of young concrete are used to predict strength evolution and this prediction is verified by independent test results using cylinders containing more mature concrete.

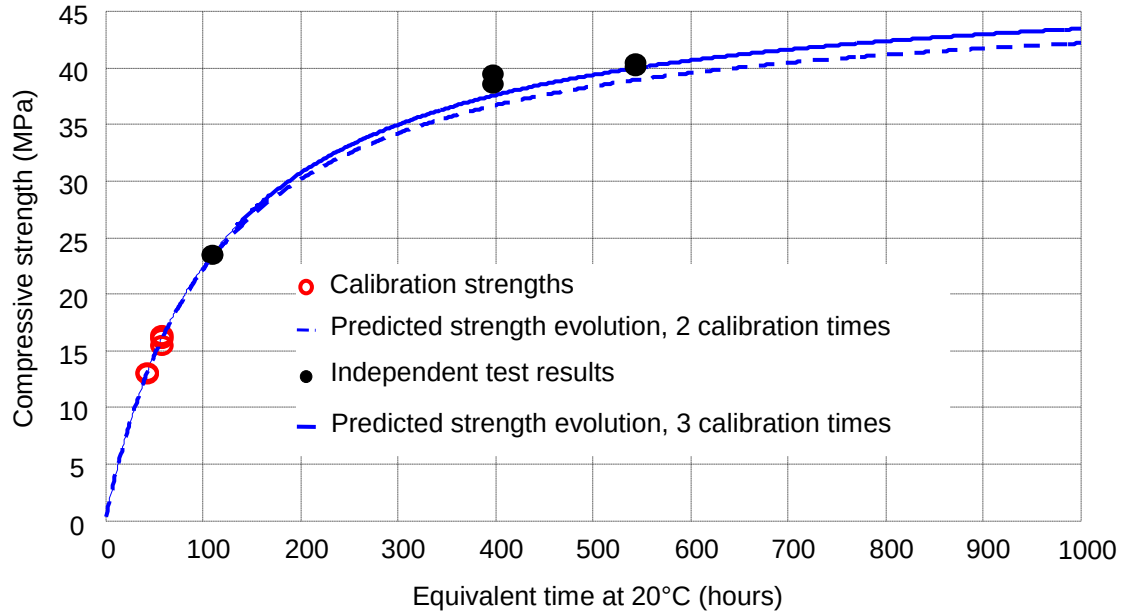

Figure 13 Compressive strength vs. equivalent time for test series 4. Calibration strengths of young concrete are used to predict strength evolution and this prediction is verified by independent test results using cylinders containing more mature concrete.

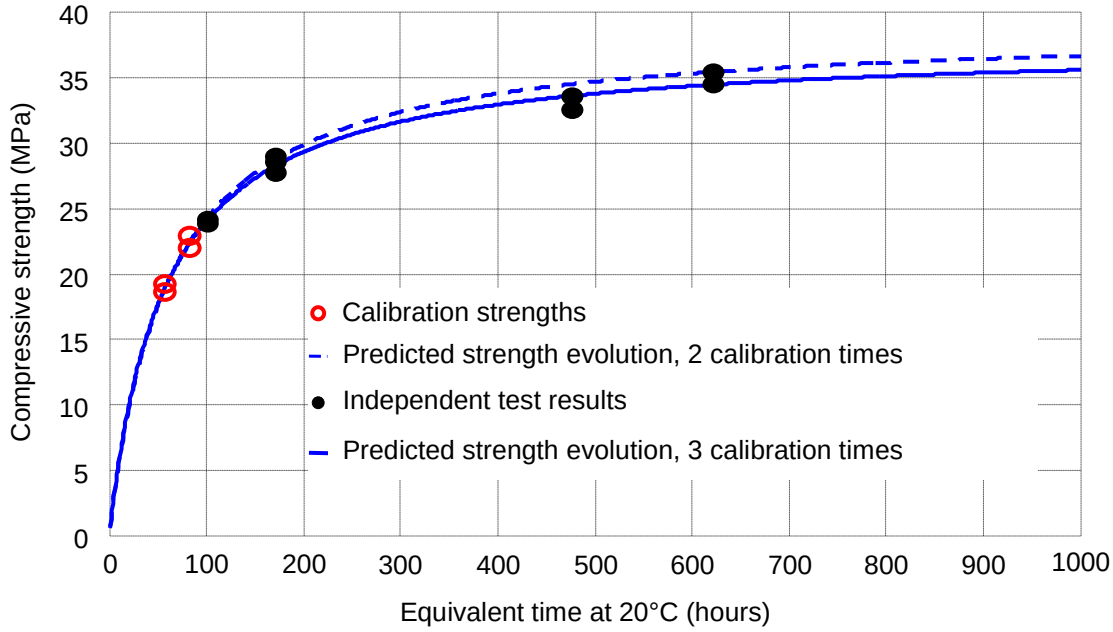

Figure 14 Compressive strength vs. equivalent time for test series 5. Calibration strengths of young concrete are used to predict strength evolution and this prediction is verified by independent test results using cylinders containing more mature concrete.

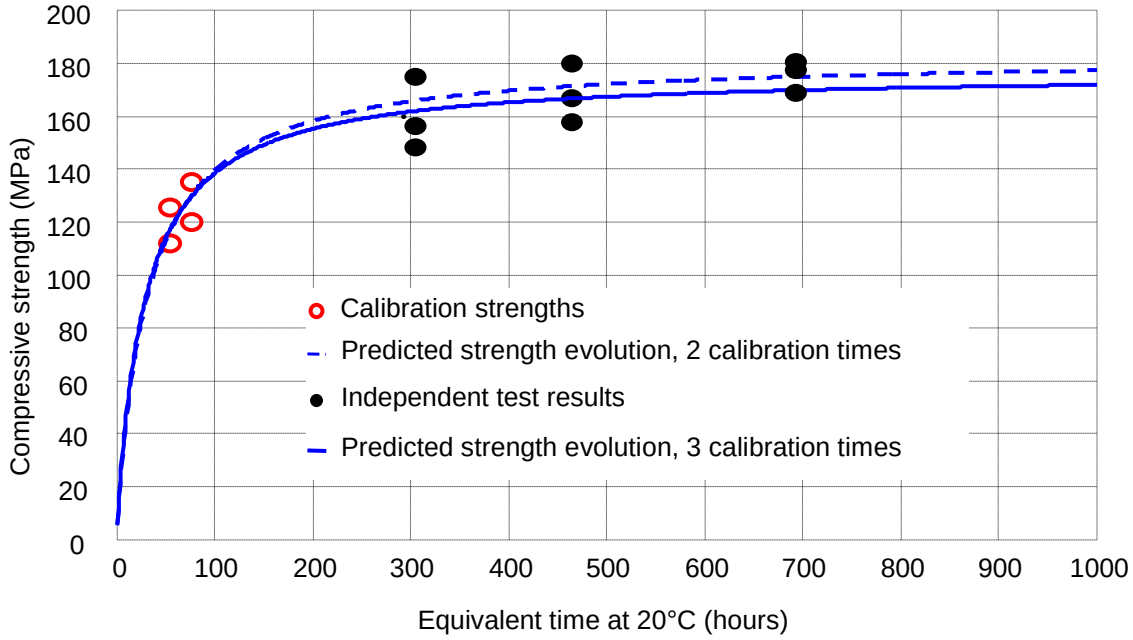

Figure 15 Compressive strength vs. equivalent time for test series 6. Calibration strengths of young concrete are used to predict strength evolution and this prediction is verified by independent test results using cylinders containing more mature concrete.

300

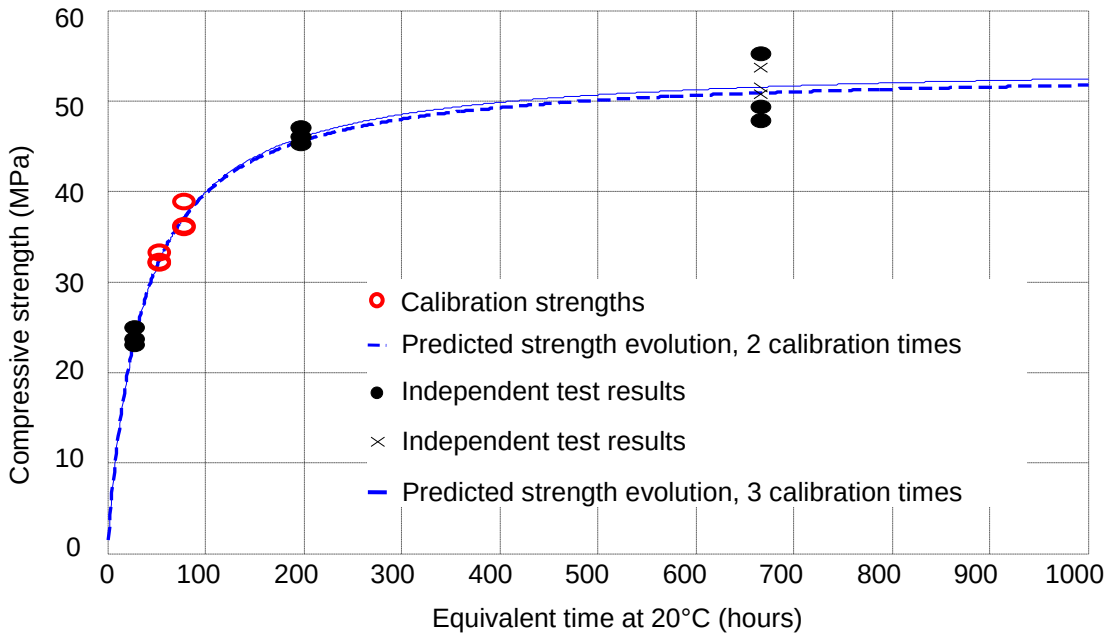

544
545 **Figure 16 Compressive strength vs. equivalent time for test series 7. Calibration strengths of**
546 **young concrete are used to predict strength evolution and this prediction is verified by**
547 **independent test results using cylinders containing more mature concrete.**
548